PROCEEDINGS of the
23rd International Congress on Acoustics
9 to 13 September 2019 in Aachen, Germany

Active control of scattering effects in 2.5D multizone reproduction

Junqing ZHANG[(1)], Wen ZHANG[(1)], Lijun ZHANG[(1)],Mengyao ZHU[(2)]

[(1)]Center of Intelligent Acoustics and Immersive Communications and School of Marine Science and Technology, Northwestern Polytechnical University, Xi'an China, E-mail: junqingzhang@mail.nwpu.edu.cn, wen.zhang@nwpu.edu.cn, zhanglj7385@nwpu.edu.cn

[(2)]School of Communication and Information Engineering, Shanghai University, Shanghai 200072, China, E-mail: zhumengyao@shu.edu.cn.

Abstract

Multizone reproduction has gained significant interest in recent years for its advantage that listeners can enjoy their personal audio without physical isolation or wearing headphones. However, study of multizone reproduction has been focused on reproducing sounds in an empty listening space. The scattering effects of the human and objects in sound zones are often neglected, causing degraded system performance. In this work, we focus on reproduction on a 2D horizontal plane using 3D secondary sources, i.e., 2.5D reproduction. Through experiments we show how scatterers such as human head and body in sound zones influence reproduction results. A modal-domain method for 2.5D multizone reproduction with an active control strategy to correct the scattering effects is proposed. The method is based on modelling the human head as a rigid sphere, based on which analytical expressions are developed to represent the scattered sound field. The method is validated through experiments using a 48-element circular loudspeaker array. Experimental results especially show the improved acoustic contrast performance using the proposed method.

Keywords: 2.5D multizone reproduction, mode matching, scatterer

1 INTRODUCTION

Nowadays, the development of multizone sound field reproduction has attracted more and more attention. It can provide a variety of different experiences for listeners in open space, such as listening to music or watching movies in specific areas, and simultaneously generating quiet regions using a single array of loudspeakers [1, 2]. It provides significant flexibility because there is no need for listeners to wear headphones or set separate isolation. Lots of methods have been proposed to achieve multizone sound field control, among which the representative ones are: acoustic contrast control (ACC) [3], pressure matching (PM) [4], the combination of ACC and PM [5] , and model-domain based reproduction [6, 7, 8]. A practical implementation is to control 2D desired fields using 3D point sources, known as 2.5D reproduction [9, 10]. Algorithms proposed in recent years have gradually evolved from single frequency based design to broadband reconstruction [11, 12]. Such improvement will promote the implementation and applications of multizone sound field reproduction.

Multizone reproduction is usually designed in an empty listening space, and most existing works assumed that there is no scatterer within the control region. In practice, the listener exists in these sound zones, producing scattered sound fields which will inevitably leak into adjacent pre-defined reproduction regions. Similar to the effects due to reverberation, the scattering effects generally degrades the reproduction performance. Experimental results proved that the scattering effects from listeners causes around 8 dB acoustic contrast loss [13]. Until now, only a few research works have been carried out to test and correct the influence of scatterers. Betlehem and Poletti [14] devised a method for sound field reproduction around a solid object in a reverberant room. Chang provided an improving control method to correct the scattering effects on the sound focused personal audio system [15]. However, both of these methods are based on multi-point control method, which requires many microphones to be placed at the control points which are uniformly placed within the sound zone. A modal-domain approach was recently developed to correct the scattering effects and achieve optimal control

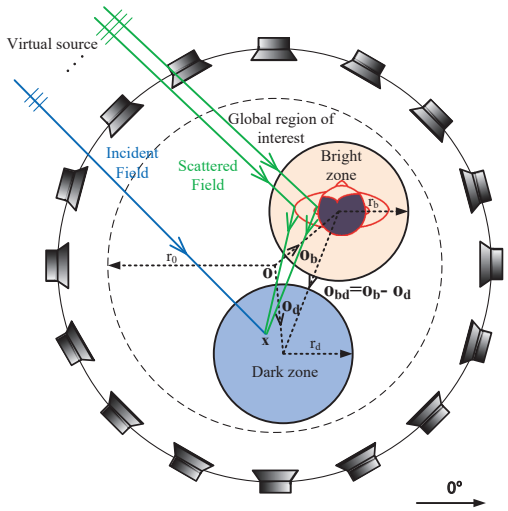

Figure 1. Geometry of multizone sound control with a scatterer inside the bright zone.

over the entire region [16]. Simulation results showed that the proposed method can improve the reproduction performance over a wide frequency range and a certain angle range in the free field environment.

The research works mentioned above are mainly base on theoretical studies and computer simulations, and very few experimental validations have been provided. In this paper, we present experimental validation of the proposed active scattered filed control in [16] using a circular loudspeaker array. In the reproduction stage, the acoustic transform function (ATF) is measured by a spherical microphone array, and the generated sound field is measured by an electret condenser microphone array in a semi-anechoic environment enclosed by acoustic baffles. In addition, the actual scattering effects and effectiveness of the active control were discussed. The remainder of this paper is organized as follows: the scattered field control theory for 2.5D multizone reproduction is revisited in Section 2. Section 3 introduces the experimental implementation of the proposed method. The experiment results and the detailed discussion are showed in Section 4. Finally, we summarize the research work in Section 5.

2 ACTIVE CONTROL OF THE SCATTERED FIELD

The geometry of multizone sound control with a scatterer inside the bright zone is shown in Figure 1. When the virtual source comes from the exterior of the control region, the sound field at an arbitrary point includes two parts: the incident field coming from the virtual source directly and the scattered field caused by the human head and body inside of the bright zone.

2.1 Sound field modal

The sound field at the observation point $\mathbf{x}$ can be represented as [16],

$$P(\mathbf{x},k) = P^{\text{in}}(\mathbf{x},k) + P^{\text{sc}}(\mathbf{x},k). \tag{1}$$

where $k = 2\pi f/c$ is the wave number with c the speed of sound and f being the temporal frequency, and superscript $(\cdot)^{\text{in}}$ and $(\cdot)^{\text{sc}}$ denote the incident field and scattered field, respectively.

2.1.1 Incident sound field

In 2.5D reproduction, the desired field is on a 2D plane, i.e., the plane is at elevation angle $\theta = \pi/2$, thus the incident sound pressure can be expressed in the form [17],

$$P^{\text{in}}(\mathbf{x},k) \approx \sum_{m=-N_0}^{N_0} \sum_{n=|m|}^{N_0} \beta_{nm}^{\text{in}}(k) j_n(k\|\mathbf{x}\|) Y_n^m e^{im\phi_{\mathbf{x}}}, \tag{2}$$

where $Y_n^m = C_n^m P_n^m(0)$ and $C_n^m = \sqrt{((2n+1)(n-|m|)!)/(4\pi(n+|m|)!)}$. $j_n(\cdot)$ is the spherical Bessel function of order n, and $\beta_{nm}^{\text{in}}(k)$ is the modal coefficient. The truncation order $N_0 = \lceil ekr_0/2 \rceil$ [18], where r_0 is the radius of the region of interest, e is the Euler's number, and $\lceil \cdot \rceil$ denotes the ceiling function. Similarly, the incident sound field at any observation point $\mathbf{x}_b \equiv (\|\mathbf{x}_b\|, \phi_{\mathbf{x}_b})$ within the bright zone can be written as,

$$P_b^{\text{in}}(\mathbf{x}_b,k) \approx \sum_{\mu=-N_b}^{N_b} \sum_{\nu=|\mu|}^{N_b} \alpha_{\nu\mu}^{\text{in}}(k) j_\nu(k\|\mathbf{x}_b\|) Y_\nu^\mu e^{i\mu\phi_{\mathbf{x}_b}}, \tag{3}$$

where $\alpha_{\nu\mu}^{\text{in}}$ is the corresponding sound field coefficients. The truncation order is $N_b = \lceil ekr_b/2 \rceil$, where r_b is the radius of the bright region.

Using the Bessel function addition formula [19], the bright zone sound field coefficients $\alpha_{\nu\mu}^{\text{in}}$ in (3) can be related to the global sound field coefficients β_{nm}^{in} in (2) as,

$$\sum_{m=-N_0}^{N_0} \sum_{n=|m|}^{N_0} \beta_{nm}^{\text{in}}(k) T_{n\nu}^{m\mu}(\mathbf{o}_b,k) = \alpha_{\nu\mu}^{\text{in}}(k), \tag{4}$$

where $\mathbf{o}_b$ is the vector that points from the global origin to the origin of the bright zone, and

$$T_{n\nu}^{m\mu}(\mathbf{o}_b,k) = 4\pi i^{\nu-n} W_1 W_2 \sum_{\ell=0}^{\infty} i^l (-1)^{2m-\mu} j_\ell(k\|\mathbf{o}_b\|) \overline{Y_{\ell(\mu-m)}}(\theta_{\mathbf{o}_b}, \phi_{\mathbf{o}_b}) \sqrt{(2n+1)(2\nu+1)(2\ell+1)/4\pi}, \tag{5}$$

with

$$W_1 = \begin{pmatrix} n & \nu & l \\ 0 & 0 & 0 \end{pmatrix}, W_2 = \begin{pmatrix} n & \nu & l \\ m & -\mu & (\mu-m) \end{pmatrix} \tag{6}$$

denoting the Wigner $3-j$ symbol, and $\overline{(\cdot)}$ represents the complex conjugate.

We can represent (4) in matrix form as,

$$\mathbf{T}_{\text{b}} \mathbf{b} = \mathbf{a}_{\text{b}}^{\text{in}}. \tag{7}$$

where $\mathbf{b} = [\beta_0^{\text{in}}, \ldots, \beta_{n^2+n+m+1}^{\text{in}}, \ldots, \beta_{(N_0+1)^2}^{\text{in}}]^T$, $\mathbf{a}_{\text{b}}^{\text{in}} = [\alpha_0^{\text{in}}, \ldots, \alpha_{1+\nu^2+\nu+\mu}^{\text{in}}, \ldots, \alpha_{(N_b+1)^2}^{\text{in}}]^T$, and $\mathbf{T}_{\text{b}}$ is the $(N_b+1)^2 \times (N_0+1)^2$ translation matrix. Similarly, the matrix $\mathbf{T}_{\text{d}}$ denotes the translation matrix from the global region to the dark zone.

2.1.2 Scattered sound field

In order to parameterize the scattered field, we model the human head as a rigid sphere. By applying the boundary condition on its surface, which is the particle velocity perpendicular to the surface is zero [17], the scattered field at the observation point $\mathbf{x}_b$ within the bright zone can be written as,

$$P_b^{\text{sc}}(\mathbf{x}_b,k) \approx \sum_{\mu=-N_h}^{N_h} \sum_{\nu=|\mu|}^{N_h} \alpha_{\nu\mu}^{\text{sc}} h_\nu^{(1)}(k\|\mathbf{x}_b\|) Y_\nu^\mu e^{i\mu\phi_{\mathbf{x}_b}}, \tag{8}$$

where $h_\nu^{(1)}(\cdot)$ represents the outing spherical Hankel functions. The scattered field modal coefficients $\alpha_{\nu\mu}^{\text{sc}}$ can be calculated using the relationship $\alpha_{\nu\mu}^{\text{sc}} = (-j_\nu'(ka)/h_\nu^{(1)'}(ka))\alpha_{\nu\mu}^{\text{in}}$, where $(\cdot)'$ denotes the corresponding derivative. The truncation order is $N_h = \lceil eka/2 \rceil$ with a the radius of the human head.

For observation points within the dark zone, the scatterer can be viewed as an exterior source. Thus, the sound pressure of the observation point $\mathbf{x}_d$ within the dark zone can be written as,

$$P_d^{\mathrm{sc}}(\mathbf{x}_d,k) \approx \sum_{u=-N_d}^{N_d} \sum_{v=|u|}^{N_d} \zeta_{vu}^{\mathrm{sc}} j_v(k\|\mathbf{x}_d\|) Y_v^u e^{iu\phi_{\mathbf{x}_d}}, \tag{9}$$

where $N_d = \lceil ekr_d/2 \rceil$, and r_d is the radius of the dark zone. Analogous to (4), based on the corresponding addition theorem for $h_v^{(1)}(k\|x_b\|)Y_v^{\mu}(\theta_{x_b},\phi_{x_b})$ [19], we have

$$\sum_{\mu=-N_h}^{N_h} \sum_{v=|\mu|}^{N_h} \alpha_{v\mu}^{\mathrm{sc}} S_{vv}^{\mu u}(\mathbf{o}_{bd},k) = \zeta_{vu}^{\mathrm{sc}}, \tag{10}$$

where

$$S_{vv}^{\mu u}(\mathbf{o}_{bd},k) = 4\pi i^{v-v} W_3 W_4 \sum_{\ell=0}^{\infty} i^l (-1)^{2\mu-u} h_\ell(k\|\mathbf{o}_{bd}\|) \overline{Y_{\ell(u-\mu)}}(\theta_{\mathbf{o}_{bd}},\phi_{\mathbf{o}_{bd}}) \sqrt{(2v+1)(2v+1)(2\ell+1)/4\pi}, \tag{11}$$

with the vector $\mathbf{o}_{bd} = \mathbf{o}_b - \mathbf{o}_d$, and W_3 and W_4 denote Wigner $3-j$ symbol.
The matrix-vector notation of (10) is

$$\mathbf{S}_{\mathrm{bd}}\mathbf{a}_{\mathrm{b}}^{\mathrm{sc}} = \mathbf{c}_{\mathrm{d}}^{\mathrm{sc}}. \tag{12}$$

where $\mathbf{a}_{\mathrm{b}}^{\mathrm{sc}} = [\alpha_0^{\mathrm{sc}},\ldots,\alpha_{v^2+v+\mu+1}^{\mathrm{sc}},\ldots,\alpha_{(N_h+1)^2}^{\mathrm{sc}}]^T$, $\mathbf{c}_d^{\mathrm{sc}} = [\zeta_0^{\mathrm{sc}},\ldots,\zeta_{v^2+v+u+1}^{\mathrm{sc}}\ldots,\zeta_{(N_d+1)^2}^{\mathrm{sc}}]^T$, and $\mathbf{S}_{\mathrm{bd}}$ is the $(N_d+1)^2\times(N_h+1)^2$ translation matric.

2.2 Modified formulation and control

In the previous work [10], we formulated the multizone reproduction problem in the modal domain as obtaining the global sound field coefficients $\mathbf{b}$ to generate a desired sound field within bright zone which characterised by its local coefficients $\mathbf{a}_{\mathrm{b}}^{\mathrm{in}}$. The energy of the dark zone and entire global sound field were set as constraints for the optimization problem. Then, we proposed a modified formulation, which reduced the energy of both the incident and scattered fields in the dark zone [16]. That is,

$$\min_{\mathbf{b}} \quad \|\mathbf{T}_{\mathrm{b}}\mathbf{b} - \mathbf{a}_{\mathrm{b}}^{\mathrm{in}}\|^2 \tag{13}$$

$$\text{subject to} \quad \|(\mathbf{T}_{\mathrm{d}} + \mathbf{R}_{\mathrm{d}})\mathbf{b}\|^2 \le e_{\mathrm{d}} \tag{13a}$$

$$\|\mathbf{b}\|^2 \le e_{\mathrm{g}}, \tag{13c}$$

According to (12), the scattering components are linked to the incident sound field and the global components, that is

$$\mathbf{c}_{\mathrm{d}}^{\mathrm{sc}} = \mathbf{R}_{\mathrm{d}}\mathbf{b} \tag{14}$$

where $\mathbf{R}_{\mathrm{d}} = \mathbf{S}_{\mathrm{bd}}\mathbf{Q}\mathbf{E}\mathbf{T}_{\mathrm{b}}$ represents the translation matrice from the bright zone to the dark zone. The matrix $\mathbf{Q} = \mathrm{diag}\big(-j_0'(ka)/h_0^{(1)'}(ka),\ldots,-j_{N_h}'(ka)/h_{N_h}^{(1)'}(ka)\big)$ is a diagonal matrix, and the matrix $\mathbf{E}$ is used to pick the first $(N_h+1)^2$ elements of the vector $\mathbf{T}_{\mathrm{b}}\mathbf{b}$ given the truncation order of the scattered field in the bright zone is N_h. Solving this constrained optimization problem, we can obtain the global coefficients $\mathbf{b}$.

2.3 2.5D weighted mode matching reproduction

The aim of the multizone sound field reproduction is to choose the loudspeaker driving signals to generate a desired sound field $P^{\mathrm{in}}(\mathbf{x},k)$ at each position $\mathbf{x}$ in the control region $\mathbb{D}$. The control region shall be circular of

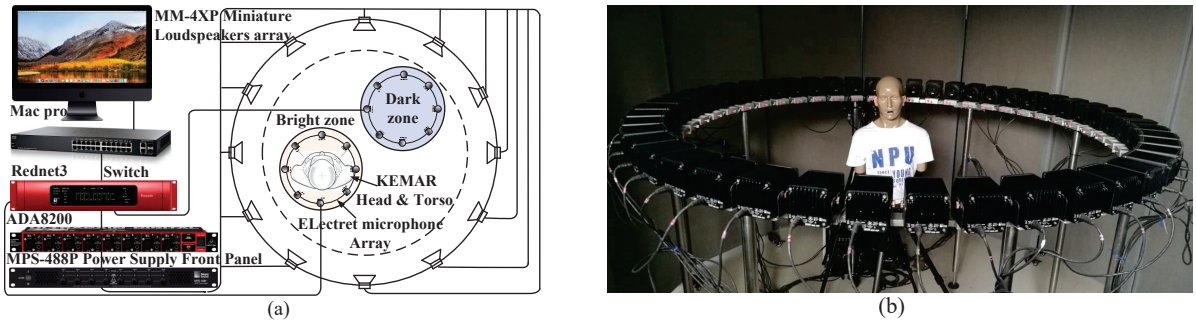

Figure 2. (a) Illustration of the setup of the 2.5D reproduction system, (b) experimental layout: A KEMAR Head and Torso Simulator is placed at the center of the bright zone within a 48-channel circular loudspeaker array in a semi-silent environment.

radius r_0 centered about the origin as shown in Figure 1. The global sound field generated by an array of L loudspeakers can be represented as,

$$P(\mathbf{x},k) = \sum_{\ell=1}^{L} d_\ell(k) G_\ell(\mathbf{x},k), \tag{15}$$

where $G_\ell(\mathbf{x},k)$ represents the ATF between the ℓth loudspeaker and the observation point $\mathbf{x}$ in the global system. d_ℓ is the ℓth loudspeaker driving signal.

We adopt the weighted mode matching approach to minimize the weighted least squares error over the entire control region [16]. By referring to (2) and (15), the cost function can be written as,

$$J(\mathbf{d},k) = \frac{1}{2\pi} \int_{\mathbb{D}} \left| P(\mathbf{x},k) - P^{\text{in}}(\mathbf{x},k) \right|^2 d\mathbf{x}. \tag{16}$$

Until now, we can obtain the loudspeaker driving signals by solving this cost function. The reader is encouraged to refer to [16] for a detailed derivation of the theory behind the design.

3 IMPLEMENTATION

As mentioned in Section 2.1.2, the proposed active scattered field control is based on assuming the human head as a rigid sphere. However, for human listeners, the effects of the scatterer are not only due to the human head, but also the human body (including shoulders, neck, and clothes, etc.). Therefore, it is necessary to validate the proposed theory on a human body, such as a head and torso simulator. The illustration of the measurement setup and experimental layout are showed in Figure 2(a) and (b), respectively.

3.1 Acoustic transform function measurement

In the reproduction stage, we measure the ATF between the loudspeakers and observation points [16] to obtain the loudspeaker driving signals. The room environments and sensor errors are very sensitive to sound field reconstruction, so the accurate measurement of ATF is very important. High order spherical microphone array is a good choice in 3D sound field coefficient extraction [20]. In our experiment setup, the global control region is a circular area of radius 1 m. Due to the limited observation range of a single microphone array, we often need a distributed microphone arrays to complete ATF measurement over this large area [21].

In our experiment, we use the MH Acoustics' Eigenmike EM32 to capture the sound pressure produced by the loudspeaker. We move a single Eigenmike along a horizontal circle (assuming stationary conditions) [21] to capture the global sound field. This strategy not only reduces the hardware costs, but also avoids perturbations

of the scattering effects when Eigenmikes are set nearby for the measurement. A five second-long exponential sweep from [20,20000] Hz frequency range is feed to each loudspeaker as an excitation signal [22].

3.2 Hardware implementation

The experiment is conducted in the Acoustics and Audio Lab at the Center of Intelligent Acoustics and Immersive Communications (CIAIC), Northwestern Polytechnical University. The measurements are performed at a sampling frequency of 48 kHz using a Dante audio interface. As shown in Figure 2(a), Dante network provides all the experimental equipments with a synchronized clock. The loudspeaker driving signals are sent by the Mac Pro to the switch, then to the sound card Focusrite Rednet3. Finally, the signals are sent to the speaker through the sound card. The Meyer Sound MM4XP miniature analog loudspeakers are powered by MPS-488P Power Supply devices, and we use the ADA8200 as the D/A converter to convert the digital driving signals to the loudspeaker analog input signal. In Figure 2(b), a circular array of 48 loudspeakers are used to synthesize sound field in a two dimensional 2D plane levelled with the listener's (or the mannequin's) ears. The GRAS 45BB KEMAR Head and Torso Simulator wearing a T-shirt is placed at the original of the local bright zone. The loudspeakers are equally spaced on a circle with a radius of 1m. The acoustic barriers enclose the circular loudspeaker array to create a semi-anechoic environment, which is used to match the simulation condition used in [16]. After the ATF encoding is completed, we send the driving signals to the loudspeaker array to reproduce the global sound field. Finally, an electret condenser microphone array is used to measure the reproduced sound field within different listening zones.

4 EXPERIMENTAL VALIDATION

In this section, we present the experimental setup and discuss the measurement results.

4.1 Experimental measurement setup

We evaluate the reproduction performance over a broadband frequency range [100,1000] Hz and angle range $[0^{\text{o}}, 180^{\text{o}}]$. The desired field is a plane wave with an amplitude of $A = 1$ coming from the azimuth angle ϕ_{pw}. For the evaluation along with frequency, the coming angle of the plane wave is $\phi_{pw} = 120^{\text{o}}$. For the evaluation along with angle, the frequency of the plane wave is 600 Hz. For both cases, we set the energy constraints in the dark zone and global region to $e_d = 0$ dB and $e_g = 20$ dB. Each sound zone has a radius of 0.15 m. The bright zone and dark zone are located at $\mathbf{o}_b = (0.4, 0)$ and $\mathbf{o}_d = (-0.4, 0)$ with respect to the global origin, respectively.

4.2 Evaluation indicator

The evaluation indicator is the acoustic contrast $\kappa(k)$ between the bright zone and dark zone,

$$\kappa(k) = 10\log_{10}\frac{\frac{1}{\mathbb{V}_b}\int_{\mathbb{D}_b}\left|P(\mathbf{x},k)\right|^2 d\mathbf{x}}{\frac{1}{\mathbb{V}_d}\int_{\mathbb{D}_d}\left|P(\mathbf{x},k)\right|^2 d\mathbf{x}} \tag{17}$$

where $P(\mathbf{x},k)$ represents the reproduced sound field at a point within the bright zone $\mathbb{D}_b$ or the dark zone $\mathbb{D}_d$. $\mathbb{V}_b$ and $\mathbb{V}_d$ denote the area of the bright zone and the dark zone, respectively.

4.3 Experiment results and discussion

We evaluate the acoustic contrast over a broadband frequency range and a certain angle range. The blue, black and red lines correspond to the case that there is no scatterer (**Incident**) [10], using the traditional method without scattered field control (**Scattered**), and using the proposed scattering control method (**Proposed**) [16]. Performance results in Figure 3(a) shows that the scattering effects of the KEMAR mannequin head and body on the reproduction performance can not be ignored, the acoustic contrast has $0.1 - 4.8$ dB loss when the

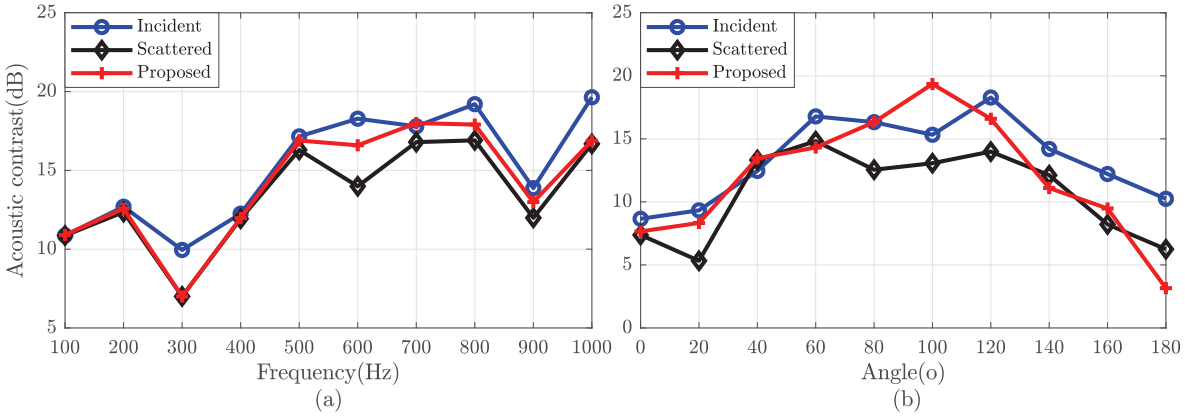

Figure 3. Acoustic contrast along with a broadband frequency range and a wide angle range.

KEMAR mannequin is inside the bright zone. Especially at 600 Hz, the acoustic contrast loss is up to 4.8 dB. Using the proposed method, about $0.1-3.1$ dB gain in acoustic contrast is achieved in the frequency range [500,1000] Hz. In Figure 3(b), the acoustic contrast has $0-3.5$ dB loss over the angle range $[0^o, 180^o]$. The proposed active control method can improve the performance within the range $[70^o, 130^o]$. It is noteworthy that there is around 6.5 dB acoustic contrast improvement at 100^o.

5 CONCLUSIONS

In this work, we presented an active control of scattering effect in 2.5D multizone reproduction with experimental validation. Based on wave modelling theory and translation theorem, we developed analytical expressions of the incident and scattered fields for the global region and each sound zone. We then proposed an active control strategy to correct the scattering effects and used the weighted mode matching approach for reproduction. The experimental results showed that the scattering effects produced by the human head and body severely degrade the reproduction performance. The proposed scattered field control method is based on the assumption of modeling the human head as a rigid sphere and can achieve acoustic control improvement over a broadband frequency and angle range. Future work will investigate incorporating the human torso scattering effect into the control and examine the proposed method in reverberant environments.

ACKNOWLEDGEMENTS

This work was supported by the National Natural Science Foundation of China (NSFC) funding scheme under Project No. 61671380.

REFERENCES

[1] T. Betlehem, W. Zhang, M. A. Poletti, and T. D. Abhayapala, "Personal sound zones: Delivering interface-free audio to multiple listeners," *IEEE Signal Processing Magazine*, vol. 32, no. 2, pp. 81–91, 2015.

[2] W. Zhang, P. Samarasinghe, H. Chen, and T. Abhayapala, "Surround by sound: A review of spatial audio recording and reproduction," *Applied Sciences*, vol. 7, no. 5, p. 532, 2017.

[3] S. J. Elliott, J. Cheer, J.-W. Choi, and Y.-H. Kim, "Robustness and regularization of personal audio systems," *IEEE Trans. Audio, Speech, Lang. Process.*, vol. 20, no. 7, pp. 2123–2133, 2012.

[4] M. A. Poletti, "An investigation of 2D multizone surround sound systems," in *Audio Eng. Soc. (AES) Conv.*, (San Francisco, USA), p. 9 pages, Oct. 2008.

[5] J.-H. Chang and F. Jacobsen, "Sound field control with a circular double-layer array of loudspeakers," *J. Acoust. Soc. Am.*, vol. 131, no. 6, pp. 4518–4525, 2012.

[6] Y. Wu and T. D. Abhayapala, "Spatial multizone soundfield reproduction: Theory and design," *IEEE Trans. Audio, Speech, Lang. Process.*, vol. 19, pp. 1711–1720, June 2011.

[7] M. A. Poletti and F. M. Fazi, "An approach to generating two zones of silence with application to personal sound systems," *J. Acoust. Soc. Am.*, vol. 137, no. 2, pp. 598–605, 2015.

[8] W. Zhang, T. D. Abhayapala, T. Betlehem, and F. M. Fazi, "Analysis and control of multi-zone sound field reproduction using modal-domain approach," *J. Acoust. Soc. Am.*, vol. 140, pp. 2134–2144, 2016.

[9] W. Zhang and T. D. Abhayapala, "2.5D sound field reproduction in higher order ambisonics," in *Proc. IEEE IWAENC*, pp. 342–346, IEEE, 2014.

[10] W. Zhang, J. Zhang, T. D. Abhayapala, and L. Zhang, "2.5D multizone reproduction using weighted mode matching," in *Proc. IEEE ICASSP*, (Calgary, Alberta, Canada), pp. 476–480, IEEE, 2018.

[11] J. Donley, C. Ritz, and W. B. Kleijn, "Multizone soundfield reproduction with privacy-and quality-based speech masking filters," *IEEE Trans. Audio, Speech, Lang. Process.*, vol. 26, no. 6, pp. 1041–1055, 2018.

[12] M. Buerger, C. Hofmann, and W. Kellermann, "Broadband multizone sound rendering by jointly optimizing the sound pressure and particle velocity," *J. Acoust. Soc. Am.*, vol. 143, no. 3, pp. 1477–1490, 2018.

[13] M. Olsen and M. B. Møller, "Sound zones: Scattering study with head and torso simulator," in *Audio Eng. Soc. (AES) Conv.*, (Guildford, USA), p. 9 pages, Sep. 2013.

[14] T. Betlehem and M. A. Poletti, "Sound field reproduction around a scatterer in reverberation," in *Proc. IEEE ICASSP*, (Taipei, China), pp. 89–92, IEEE, 2009.

[15] J.-H. Chang, J.-Y. Park, and Y.-H. Kim, "Scattering effect on the sound focused personal audio system," *J. Acoust. Soc. Am.*, vol. 125, no. 5, pp. 3060–3066, 2009.

[16] J. Zhang, W. Zhang, T. D. Abhayapala, J. Xie, and L. Zhang, "2.5D multizone reproduction with active control of scattered sound fields," in *Proc. IEEE ICASSP*, (Brighton, UK), pp. 141–145, May 2019.

[17] E. G. Williams, *Fourier Acoustics: Sound Radiation and Nearfield Acoustical Holography*. San Diego, CA: Academic Press, pp. 334-232, 1999.

[18] R. A. Kennedy, P. Sadeghi, T. D. Abhayapala, and H. M. Jones, "Intrinsic limits of dimensionality and richness in random multipath fields," *IEEE Transa. Signal Process.*, vol. 55, pp. 2542–2556, June 2007.

[19] P. A. Martin, *Multiple scattering: interaction of time-harmonic waves with N obstacles*. No. 107, Cambridge University Press, pp.87-90, 2006.

[20] P. N. Samarasinghe, T. D. Abhayapala, and M. A. Poletti, "Synthesis of room transfer function over a region of space by multiple measurements using a higher-order directional microphone," in *Proc. IEEE ChinaSIP*, pp. 6–10, IEEE, 2014.

[21] Y. Hu, P. N. Samarasinghe, G. Dickins, and T. D. Abhayapala, "Modeling the interior response of real loudspeakers with finite measurements," in *Proc. IEEE IWAENC*, pp. 16–20, IEEE, 2018.

[22] M. Binelli, A. Venturi, A. Amendola, and A. Farina, "Experimental analysis of spatial properties of the sound field inside a car employing a spherical microphone array," in *Audio Eng. Soc. (AES) Conv.*, Audio Engineering Society, 2011.